*Article*

# Precipitation of Ferrous Oxalate from Ferrous Ammonium Sulfate in Oxalic Acid Solution

**Su In Lee** [1], **Hye Rim Kim** [1], **Jae Kwan Park** [1], **Wonzin Oh** [2,*], **Jeongju Kim** [3], **Chorong Kim** [3], **Junghyun Lee** [4], **Ki-Chul Kim** [4] and **Byung-Chul Lee** [1,*]

[1] Department of Chemical Engineering, Hannam University, Daejeon 34054, Republic of Korea
[2] Research Institute of Advanced Energy Technology, Kyungpook National University, Daegu 41566, Republic of Korea
[3] KHNP Central Research Institute, Daejeon 34101, Republic of Korea
[4] KEPCO KPS, Busan 46036, Republic of Korea
* Correspondence: wonzin@knu.ac.kr (W.O.); bclee@hnu.kr (B.-C.L.); Tel.: +82-42-629-8838 (B.-C.L.)

**Abstract:** A kinetic study was conducted experimentally for the precipitation of ferrous oxalate. The ferrous oxalate, in the form of dihydrate ($FeC_2O_4 \cdot 2H_2O$), was produced by the acidic dissolution of ferrous ammonium sulfate ($Fe(NH_4)_2(SO_4)_2$) in an aqueous solution of oxalic acid, and then precipitated by nucleation and particle growth from supersaturated solution. The effect of the concentration of ferrous ammonium sulfate and oxalic acid as raw materials was investigated on the kinetics of the ferrous oxalate precipitation. Temperature was kept constant at 25 °C. The surface morphology, atomic compositions, and crystal phase were characterized for the ferrous oxalate precipitate collected. As the initial concentration of ferrous ammonium sulfate increased, the initial precipitation of ferrous oxalate occurred faster. The concentration of oxalic acid did not significantly affect the rate of precipitation of ferrous oxalate. The experimental behavior of ferrous oxalate precipitation was modeled with first-order models of reaction kinetics.

**Keywords:** precipitation; ferrous oxalate; ferrous ammonium sulfate; oxalic acid; kinetics; chemical decontamination

## 1. Introduction

Radioactive materials produced in the reactor of a nuclear power plant (NPP) are deposited as corrosion oxide layers inside the primary coolant system. The corrosion oxides, deposited with radionuclides, are mainly metal oxides of iron, nickel, and chromium. It is essential to lower a radioactivity level by removing the corrosion oxides using a decontamination method before decommissioning [1,2]. Among various decontamination methods, chemical decontamination is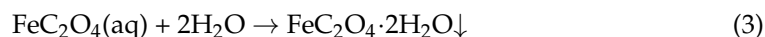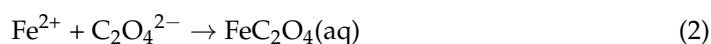 a main technology that is capable of removing more than 95% of radionuclides generated in the primary coolant system. An extensive survey of the status and prospects of various decontamination and decommissioning technologies has recently been reported [3].

Chemical decontamination, which has been considered the most effective method so far, involves dissolving the corrosion metal oxides using redox reactions [4–9]. In order to dissolve magnetite ($Fe_3O_4$), a typical corrosion oxide, through a reductive reaction, decontamination processes developed using oxalic acid have generated the most interest [6,7]. Recently, Lee and Oh [1] studied the temperature and concentration dependencies of chemical equilibrium for reductive dissolution of magnetite using oxalic acid. Kim et al. [2] reported kinetic experimental data on the reductive dissolution of a synthetic magnetite specimen using an aqueous oxalic acid solution.

The reaction schemes of the reductive dissolution of magnetite by oxalic acid are well known as follows [1]:

$$Fe_3O_4 + 4H_2C_2O_4 \rightarrow 3Fe^{2+} + 3C_2O_4^{2-} + 2CO_2(g) + 4H_2O \tag{1}$$

$$Fe^{2+} + C_2O_4^{2-} \rightarrow FeC_2O_4(aq) \tag{2}$$

$$FeC_2O_4(aq) + 2H_2O \rightarrow FeC_2O_4 \cdot 2H_2O\downarrow \tag{3}$$
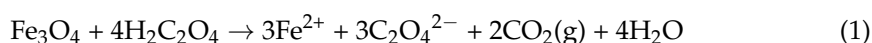
Oxalic acid, a strong reducing agent, transfers electrons to $Fe^{3+}$ ions to be reduced to $Fe^{2+}$ ions. The complex formation of the dissolved ferrous ions with the oxalate according to reaction (2) produces ferrous oxalate. Ferrous oxalate exists in the form of dehydrate, as given in reaction (3). When the concentration of ferrous oxalate in the aqueous solution exceeds its solubility in water, the dissolved ferrous oxalate precipitates in the form of small particles. The precipitates thus formed are prone to be deposited inside the NPP coolant system and can be recovered with difficulty.

The purpose of this study is to investigate the kinetic behavior of the precipitation of ferrous oxalate. When $Fe_3O_4$ is dissolved by oxalic acid, ferric ions ($Fe^{2+}$) reduced from ferrous ions ($Fe^{3+}$) by oxalic acid are combined with oxalate anions to form ferrous oxalate. Since the reduction reaction and crystal growth occur sequentially, the crystal growth and subsequent precipitation of ferrous oxalate occur very slowly and for a long time. This makes it difficult to observe the precipitation behavior of ferrous oxalate. As a result of searching for a material that provides the ferrous ions as a substitute for magnetite, ferrous ammonium sulfate ($Fe(NH_4)_2(SO_4)_2$) was considered for this study. Dissolution of ferrous ammonium sulfate by oxalic acid occurs very quickly, and crystal growth and precipitation also occur rapidly, which can be considered suitable for kinetics studies. The precipitation of ferrous oxalate is performed by the chemical reaction in aqueous solution between ferrous ammonium sulfate and oxalic acid:

$$Fe(NH_4)_2(SO_4)_2 + H_2C_2O_4 \rightarrow FeC_2O_4 + 2NH_4^+ + 2SO_4^{2-} + 2H^+ \tag{4}$$
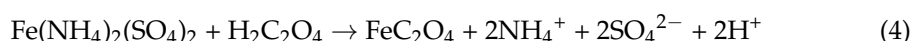
Figure 1 shows the comparison of the chemical equilibrium calculations for two different dissolution systems: (a) the reductive dissolution of a magnetite ($Fe_3O_4$) in an aqueous solution of oxalic acid; (b) a simple dissolution of ferrous ammonium sulfate ($Fe(NH_4)_2(SO_4)_2$) powder in oxalic acid. The calculations were performed using Visual MINTEQ ver. 3.1 software. The profiles of the equilibrium concentrations for the two systems according to the change in the initial concentration of $Fe^{2+}$ showed many similarities in the behavior of the concentrations of $Fe^{2+}$ and ferrous oxalate complex. The pH changes for the two systems also showed similar behavior. Therefore, in this study, it was decided to use ferrous ammonium sulfate as a raw material for producing ferrous oxalate. After rapidly dissolving ferrous ammonium sulfate powder in oxalic acid, experiments for the precipitation of ferrous oxalate were carried out.

There have been many studies on the formation and precipitation of ferrous oxalate. Müller et al. [10] obtained ferrous oxalate dihydrate ($\alpha$-FeC$_2$O$_4 \cdot 2H_2O$) in the form of yellow–brownish single crystal precipitate by dissolving iron in sulfuric acid and reacting it with dimethyl oxalate. Li et al. [11] demonstrated ferrous oxalate precipitation by the chemical reaction between ferrous sulfate and oxalic acid and studied the nucleation and crystal growth kinetics of ferrous oxalate with a turbidity measurement, classical nucleation and particle growth theory. The nucleation rate was presented in relation to the degree of supersaturation, and the grain growth rate was presented as a function of the difference between the particle surface and bulk concentration of ferrous oxalate. Abdel-Ghafar et al. [12–14] studied nucleation fundamentals and morphologies of ferrous oxalate dihydrate crystals in deionized water and diluted phosphoric acid media. Ferrous sulfate heptahydrate crystals and oxalic acid were mixed in deionized water and diluted phosphoric acid. The turbidity of the mixture at different time intervals was measured and the induction time was calculated for ferrous oxalate dihydrate crystals. Xiao et al. [15] proposed a liquid-phase oxalate coprecipitation method to produce ferropericlase ($Mg_{0.8}Fe_{0.2}O$) by adding oxalic acid to a mixed solution of ferrous sulfate and magnesium chloride.
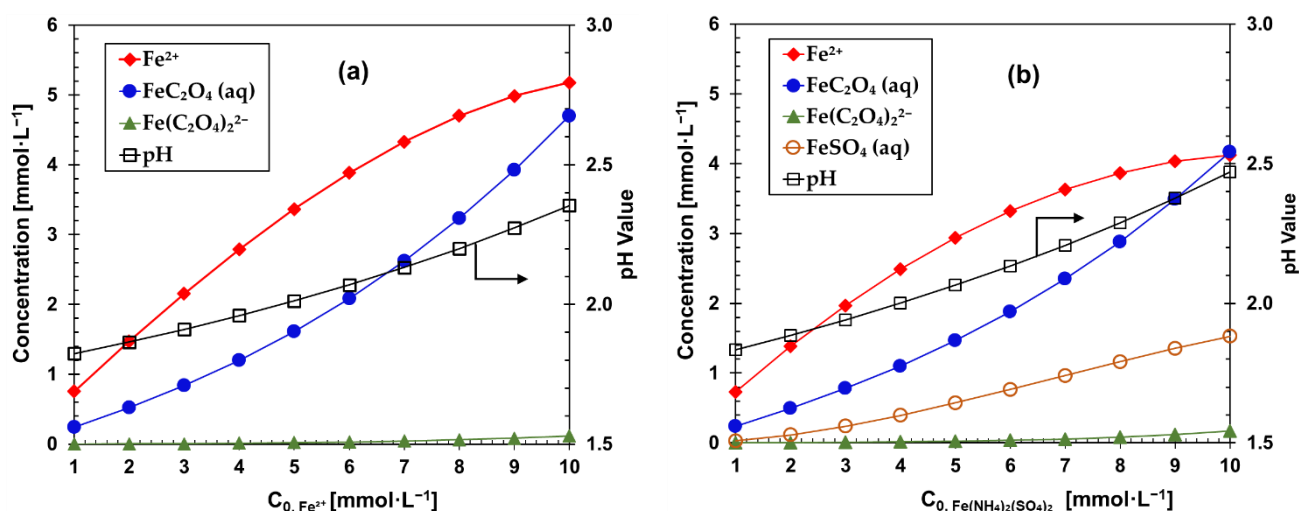
**Figure 1.** Comparison of the equilibrium calculations of ferrous oxalate concentration for two different dissolution systems at a constant oxalic acid concentration of 20 mmol·L$^{-1}$ and at 25 °C: (**a**) reductive dissolution of Fe$_3$O$_4$; (**b**) simple dissolution of Fe(NH$_4$)$_2$(SO$_4$)$_2$ powder.

Santawaja et al. [16] carried out dissolution experiments on iron oxide highly loaded in an oxalic acid aqueous solution. Highly acidic oxalic acid solution for dissolving the highly loaded iron oxide made it possible to produce an iron oxalates aqueous solution. Although Fe$_3$O$_4$ had an advantage in terms of the dissolution rate, it gave relatively low iron recovery from the solution (80~90%), which was attributed to the unavoidable formation of FeC$_2$O$_4$·2H$_2$O precipitates. Ghasemi et al. [17] developed an equilibrium oxalate precipitation diagram using the solubility product data for several metal oxalates. The precipitation experiments were performed for a synthetic sulfate solution containing the metal cations selected. Selective oxalate precipitation of the metal cations including Fe$^{2+}$ was experimentally evaluated.

Many of the studies published in the aforementioned literature are mainly on the precipitation behavior from the point of nucleation and particle growth of supersaturated solution. However, this work is intended to investigate the quantitative characteristics of precipitation behavior according to concentration to control the occurrence of ferrous oxalate precipitate in the oxalic acid solution. The concentrations of ferrous ion and oxalic acid in aqueous solution were considered as experimental parameters. Temperature was kept constant at room temperature (25 °C).

## 2. Experimental

### 2.1. Materials

Ferrous ammonium sulfate hexahydrate (Fe(NH$_4$)$_2$(SO$_4$)$_2$·6H$_2$O: CAS no. 7783-85-9) with 99% purity, purchased from Samchun Chemicals (Pyeongtaek, Republic of Korea), was used as a source that provided ferrous ions. Oxalic acid dihydrate (H$_2$C$_2$O$_4$·2H$_2$O: CAS no. 6153-56-6) with 99.5% purity for dissolving ferrous ammonium sulfate was obtained from Daejung Chemicals and Metals (Siheung, Republic of Korea). In all experiments, deionized water was used to prepare aqueous solutions and analyze samples.

### 2.2. Characterization and Analysis

The precipitate sample collected from the aqueous solution was dried at 100 °C for about four hours using a muffle furnace. The surface morphology and atomic composition of the precipitate samples were analyzed using a field emission scanning electron microscope (FE-SEM) (Jeol model JSM-7610F Plus) equipped with an energy-dispersive X-ray spectroscope (EDS). For the FE-SEM analysis, platinum coating was applied to the precipitate sample and the accelerating voltage used for imaging was 15 kV. When measuring the

atomic composition, an area-scan method was used. The crystal structure and phase of the precipitate sample were identified with X-ray diffraction (XRD) (Bruker model D2 PHASER XE-T) using a Cu-K$\alpha$ radiation source ($\lambda$ = 1.54184 Å). The step size was 0.01°, the scan speed was 2.25°·min$^{-1}$, and the counting time for each step was 0.2 s. The slit widths were set as follows: Soller slit of 0.04 radian, divergence slit of 1 mm, and matching anti-scatter slit of 3 mm. The diffractograms were recorded from 10° to 60°, and matched to reference data in the JCPDS database. The concentration of total Fe dissolved in the solution samples collected during the kinetic experiments of precipitation was determined by an inductively coupled plasma mass spectrometer (ICP-MS) (Perkin Elmer model NexION 2000), which had a detection limit of 1.5 ng·L$^{-1}$ or less for $^{56}$Fe element.

### 2.3. Apparatus and Procedure

Figure 2 shows a schematic diagram of the experimental apparatus for the kinetic experiments of the ferrous oxalate precipitation. Precipitation experiments were carried out in a cylinder-shaped 3-neck glass reactor with dimensions of 100 mm internal diameter and 150 mm height. There were no baffles installed inside the reactor. A heating and stirring mantle (MTOPS model MS-DMSDB634) was used for mixing and heating the solution and keeping the temperature of the solution constant. A thermocouple and a magnetic bar inserted into the reactor were coated with Teflon to prevent corrosion by oxalic acid solution. A reflux condenser was attached to the top of the reactor to prevent evaporation of the aqueous solution.
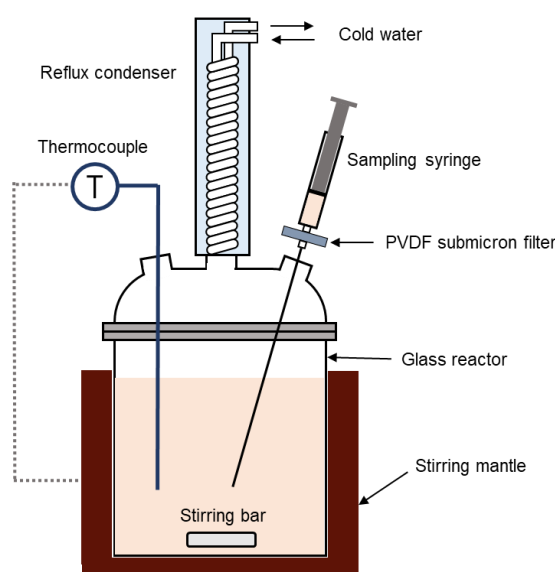


**Figure 2.** A schematic diagram of the experimental apparatus for precipitation reaction of ferrous oxalate in oxalic acid aqueous solution.

The experimental procedure is briefly described below. After setting an experimental condition first, the amounts of ferrous ammonium sulfate, oxalic acid, and deionized water were quantified by using precision balances (AND model HM-300 with ±0.1 mg accuracy and AND model GX-1003A with ±1 mg accuracy). After putting the prepared oxalic acid solution and ferrous ammonium sulfate solution into the reactor, the reflux condenser was connected. The temperature of the reactor was set by using a stirring mantle (Misung Scientific model MS-DMSDB634, Yangju, Republic of Korea) and was controlled within ±1 °C. The solution was stirred at a constant rate of 300 rpm during the reaction.

During the kinetic precipitation reaction experiment, samples were taken at fixed time intervals. After taking a sample using a syringe coupled with a submicron filter (Hyundai Micro, Seoul, Republic of Korea) of 0.2 μm polyvinylidene fluoride, it was immediately placed in a 15 mL centrifuge conical tube made of polypropylene (Hyundai Micro, Seoul,

Republic of Korea) and diluted to a concentration of 1 mmol·L$^{-1}$ or less to prevent further precipitation reaction. After separating the solid from the diluted solution using a centrifuge (ALLforLAB model ACF-10, Seoul, Republic of Korea), the supernatant was collected with a filter syringe. The reaction proceeded for a total time of 240 min to obtain kinetic data on the precipitation. As a final step, the concentration of the total Fe present in the sampled solution was determined by the ICP-MS analysis.

Table 1 gives the experimental conditions for the precipitation reaction of ferrous oxalate from the ferrous ammonium sulfate in the oxalic acid aqueous solution. The amount of the ferrous ion (Fe$^{2+}$) varied depending on the change of the concentration of ferrous ammonium sulfate introduced into the reactor. The behavior of precipitated ferrous oxalate was observed by changing the concentrations of oxalic acid. The temperature of the precipitation reaction was kept constant at 25 °C.

**Table 1.** Experimental conditions for the precipitation reaction of ferrous oxalate in oxalic acid aqueous solution.

| Operating Variable | Experimental Condition |
|---|---|
| Precipitation temperature, $T$ [°C] | 25 |
| Concentration of oxalic acid, $C_{OA}$ [mmol·L$^{-1}$] | 40, 60, 80 |
| Concentration of ferrous ammonium sulfate, $C_{FAS}$ [mmol·L$^{-1}$] | 2, 8, 16 |
| Volume of reaction solution, $V$ [mL] | 300 |
| Reaction time, $t$ [min] | 240 |

## 3. Results and Discussion

### 3.1. Characteristics of Precipitate

Figure 3 shows the FE-SEM images for the ferrous oxalate precipitate obtained from our experiments. It can be seen that the ferrous oxalate precipitate is rod- or pillar-shaped. As the initial concentration of ferrous ammonium sulfate increased, the volume and cross-sectional area of the precipitate particles increased due to the particle growth. Figure 4 shows the EDS analysis for the precipitate sample, in which the presence of Fe, C and O is indicated. According to the EDS analysis, the precipitate sample turned out to be a material with the chemical formula of Fe$_{1.00}$C$_{1.93}$O$_{4.47}$. Considering the error of analysis, it can be said that this material gives a chemical formula very close to that of ferrous oxalate (FeC$_2$O$_4$).
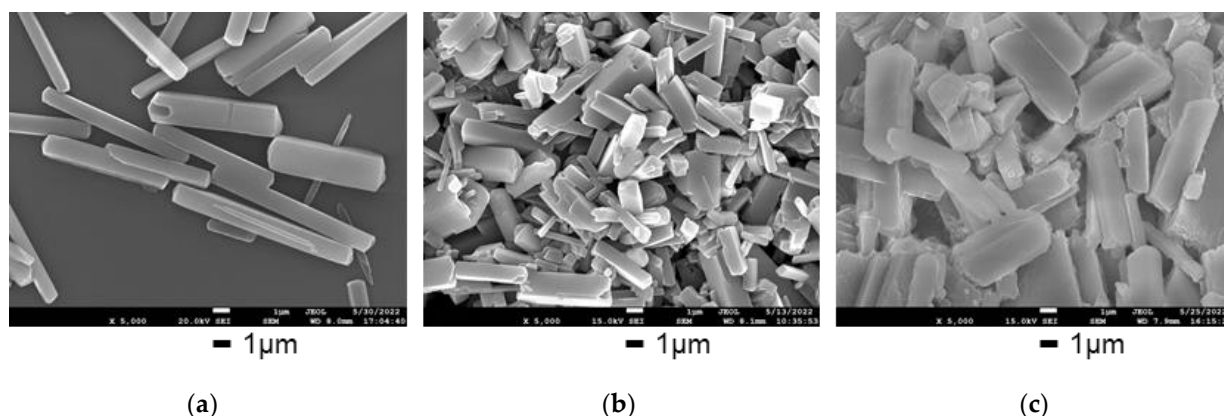


**Figure 3.** FE-SEM images (×5000 magnification) of the samples precipitated at different concentrations of ferrous ammonium sulfate ($C_{FAS}$) of 4, 16 and 30 mmol·L$^{-1}$. The oxalic acid concentration and reaction temperature were kept constant at 60 mmol·L$^{-1}$ and 25 °C, respectively. (**a**) $C_{FAS}$ = 4 mmol·L$^{-1}$; (**b**) $C_{FAS}$ = 16 mmol·L$^{-1}$; (**c**) $C_{FAS}$ = 30 mmol·L$^{-1}$.
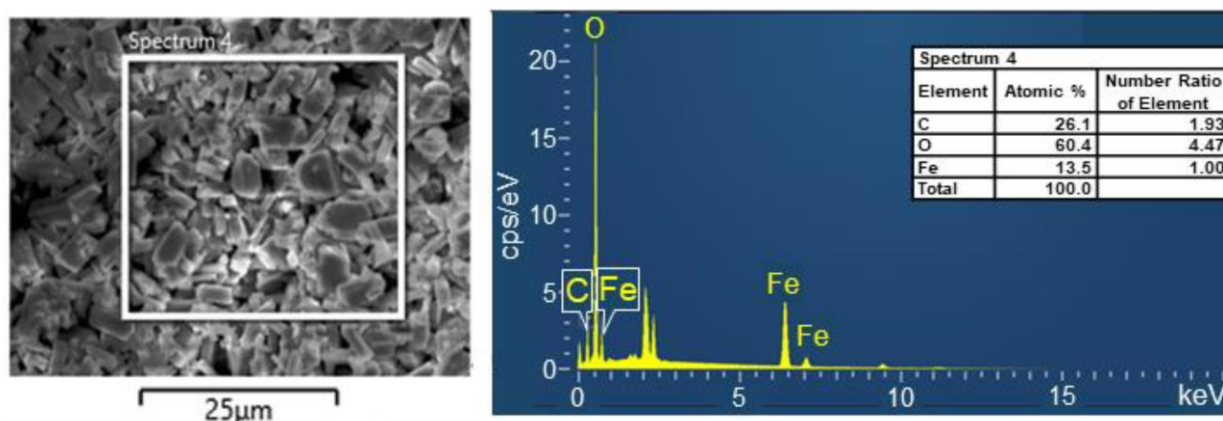
**Figure 4.** EDS analysis result of the precipitate sample. The ferrous ammonium sulfate concentration, the oxalic acid concentration, and the reaction temperature were 30 mmol·L$^{-1}$, 60 mmol·L$^{-1}$, and 25 °C, respectively.

Figure 5a shows the XRD pattern of a precipitate sample obtained in the precipitation experiment of this study, while Figure 5b shows the XRD characteristic reflections of the standard β-FeC$_2$O$_4$·2H$_2$O (JCPDS No. 22-0635) belonging to the orthorhombic crystal system. For the precipitate sample, strong reflections were detected at 2θ = 18.32°, 23.04°, 28.98°, and 34.30°. Comparing Figures 5a and 5b, it can be seen that all the diffraction reflections of the precipitate sample are indexed to those of the standard β-FeC$_2$O$_4$·2H$_2$O. Therefore, the precipitate obtained in this study was found to be β-FeC$_2$O$_4$·2H$_2$O.
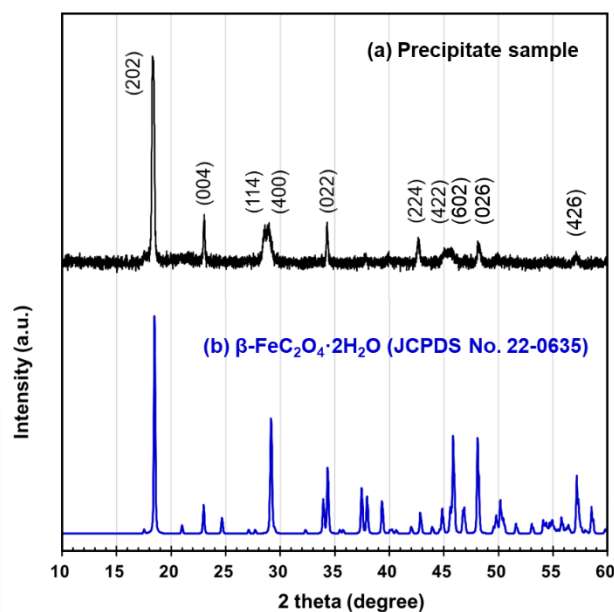


**Figure 5.** XRD patterns of (**a**) the precipitate sample obtained in this work, (**b**) standard β-FeC$_2$O$_4$·2H$_2$O (JCPDS No. 22-0635).

*3.2. Effect of the Concentration of Ferrous Ammonium Sulfate and Oxalic Acid on the Kinetics of Ferrous Oxalate Precipitation*

A kinetic study of the precipitation of ferrous oxalate was conducted with the experimental conditions of Table 1. The main experimental variables were the concentration of both ferrous ammonium sulfate and oxalic acid. During the precipitation reaction, samples of about 1 mL were taken from the reaction solution at preset reaction times, and the residual Fe content in the solution (based on concentration) was analyzed.

Figure 6 shows the residual concentration of ferrous ions ($C_{Fe^{2+}}$) as the precipitation rate of ferrous oxalate changes according to the initial concentration of ferrous oxalate. The concentration of ferrous ammonium sulfate ($C_{FAS}$) varied at 2, 8, and 16 mmol·L$^{-1}$. The concentration of oxalic acid ($C_{OA}$) and the reaction temperature were fixed at 60 mmol·L$^{-1}$ and 25 °C, respectively. Four experiments were performed under each experimental condition, and the experimental point at each reaction time is the average of the concentration values for the four experiments. In addition, the error bar showing the standard deviation for each concentration was also inserted. Noticeable changes in kinetics were observed with the change of $C_{FAS}$. When $C_{FAS}$ was 16 mmol·L$^{-1}$, the concentration of ferrous ions remaining in the reaction solution dropped sharply at the beginning of the reaction, and after that, the rate of decrease was gradually reduced and the concentration reached about 1.5 mmol·L$^{-1}$, which approached the solubility of ferrous oxalate (0.097 g of FeC$_2$O$_4$·2H$_2$O/100 mL at 25 °C; data obtained from reference [18]). This shows that the precipitation reaction of ferrous oxalate occurred very rapidly at the beginning of the reaction. Additionally, as the solubility of ferrous oxalate was reached, the precipitation reaction no longer occurred.
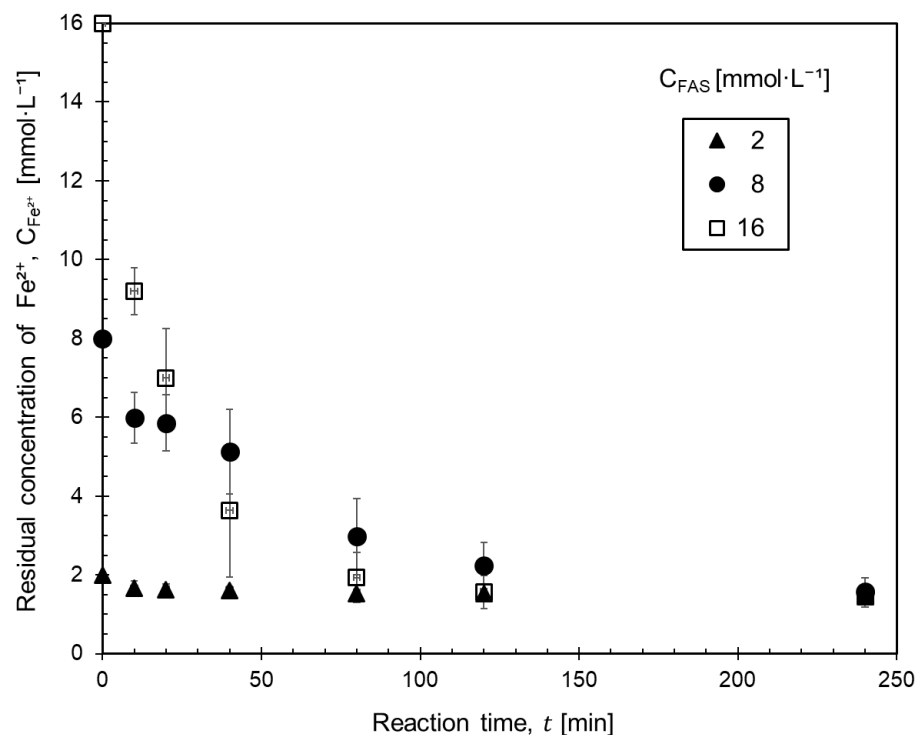


**Figure 6.** Effect of the concentration of ferrous ammonium sulfate ($C_{FAS}$) on the precipitation behavior of ferrous oxalate at $C_{OA}$ = 60 mmol·L$^{-1}$ and 25 °C.

Figure 7 shows the experimental kinetic data of ferrous oxalate precipitation according to the change of oxalic acid concentration at 25 °C. It gives the residual concentration of ferrous ions remaining in the solution without precipitation as the reaction proceeded. Note that the oxalic acid concentration ($C_{OA}$) varied at 40, 60, and 80 mmol·L$^{-1}$, while the concentration of ferrous ammonium sulfate ($C_{FAS}$) was fixed at 16 mmol·L$^{-1}$. Figure 7 represents the effect of oxalic acid concentration on the precipitation rate of ferrous oxalate. It can be seen that the precipitation behavior (the change in the precipitation rate) of ferrous oxalate in the oxalic acid concentration range set in our experiments is almost similar. That is, the concentration of oxalic acid did not significantly affect the precipitation behavior of ferrous oxalate.
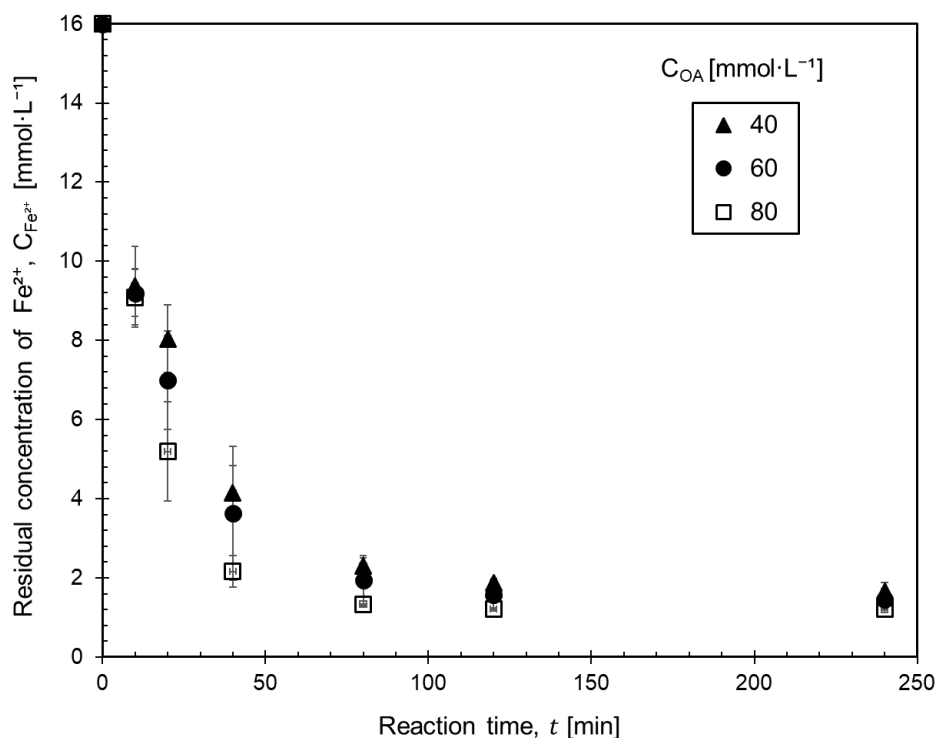
**Figure 7.** Effect of the concentration of oxalic acid ($C_{OA}$) on the precipitation behavior of ferrous oxalate at $C_{FAS}$ = 16 mmol·L$^{-1}$ and 25 °C.

### 3.3. Modeling of Ferrous Oxalate Precipitation Behavior

The supersaturated aqueous ferrous oxalate solution precipitates until the ferrous oxalate concentration reaches the solubility in aqueous phase. Therefore, the precipitation behavior of supersaturated ferrous oxalate can be simulated with a model for decreasing the residual $Fe^{2+}$ concentration. Two models for the residual $Fe^{2+}$ concentration change were adopted in this work. Model 1 is a simple first-order reaction model proportional to the residual $Fe^{2+}$ concentration, and model 2 is a model in which a reaction rate constant changes during the reaction. The residual $Fe^{2+}$ concentration in the solution as a function of time is defined as follows:

$$C_{Fe^{2+}}(t) = C^*_{FeC_2O_4} + \left( C_{Fe^{2+}} - C^*_{FeC_2O_4} \right) \tag{5}$$

where $C_{Fe^{2+}}(t)$ is the residual $Fe^{2+}$ concentration in the reaction solution and $C^*_{FeC_2O_4}$ is a solubility of ferrous oxalate that is a function of oxalic acid concentration and temperature.

The model 1 can be expressed as follows:

$$-\frac{dC_{Fe^{2+}}(t)}{dt} = k\left( C_{Fe^{2+}} - C^*_{FeC_2O_4} \right) \tag{6}$$

with an initial condition of $C_{Fe^{2+}}(0) = C_{0,Fe^{2+}} - C^*_{FeC_2O_4}$. In Equation (6), $k$ is a first-order reaction constant. Solving Equation (6) gives the following solution:

$$C_{Fe^{2+}}(t) = C^*_{FeC_2O_4} + \left( C_{Fe^{2+}} - C^*_{FeC_2O_4} \right)e^{-kt} \quad \text{where } k = \frac{\ln 2}{h} \tag{7}$$

Meanwhile, model 2 can be expressed as follows:

$$-\frac{dC_{Fe^{2+}}(t)}{dt} = k_f(1-w)\left( C_{Fe^{2+}} - C^*_{FeC_2O_4} \right) + k_s w\left( C_{Fe^{2+}} - C^*_{FeC_2O_4} \right) \tag{8}$$

where $k_f$ and $k_s$ are reaction constants for the two-parameter model. Solving Equation (8) gives the following solution:

$$C_{\mathrm{Fe}^{2+}}(t) = C_{\mathrm{FeC_2O_4}}^* + \left(C_{\mathrm{Fe}^{2+}} - C_{\mathrm{FeC_2O_4}}^*\right)\left[(1-w)e^{-k_f t} + we^{-k_s t}\right] \mathrm{where} k_f = \frac{\ln 2}{h_f} \text{ and } k_s = \frac{\ln 2}{h_s} \tag{9}$$

In Equation (7), the first-order reaction constant, $h$, represents the half-life time of the initial $\mathrm{Fe}^{2+}$ concentration, $C_{0,\mathrm{Fe}^{2+}}$. Additionally, $h_f$ and $h_s$ in Equation (9) represent the half-life times of $(1-w)C_{0,\mathrm{Fe}^{2+}}$ subject to a fast precipitation fraction and $wC_{0,\mathrm{Fe}^{2+}}$ subject to a slow precipitation fraction, respectively. The model parameters ($h$, $h_f$, $h_s$) were obtained by minimizing the sum of the square value ($F$) of the difference between the experimental value and the model calculation value as shown below:

$$F = \sum_i \left[C_{\mathrm{Fe}^{2+}}^{\exp}(i) - C_{\mathrm{Fe}^{2+}}^{\mathrm{calc}}(i)\right]^2 \tag{10}$$

Here, $w$, a weighting factor, was selected as a value that minimizes the root mean square error (RMSE) by arbitrarily setting 0.1, 0.2, 0.3, and 0.4.

The experimental results of the ferrous oxalate precipitation behavior in Figure 6 were simulated by the model Equations (7) and (9), and the results are summarized in Table 2. From the above results, it can be seen that both the model constants are the same, except when the initial concentration is low close to the solubility, so that both can be simulated by the simple first-order model Equation (7).

**Table 2.** Modeling results of the ferrous oxalate precipitation behavior for two initial concentrations of ferrous ions ($C_{0,\mathrm{Fe}^{2+}}$) of 8 and 16 mmol·L$^{-1}$ by using the ferrous ammonium sulfate system at $C_{OA}$ = 60 mmol·L$^{-1}$ and 25 °C.

| $C_{0,Fe^{2+}}$ [mmol·L$^{-1}$] | Model Parameters | | | RMSE for Two Parameter Model |
| --- | --- | --- | --- | --- |
| | $h$ | $h_f$ | $h_s$ | |
| 8 | 45 | 24.4 | 80,000 | 0.67 |
| 16 | 15 | 10.2 | 100 | 0.40 |

Figure 8 shows the comparison between the experimental results and the modeling results for the ferrous oxalate precipitation. From the modeling results, it can be seen that the precipitation behavior for most of the supersaturated ferrous oxalate solution can be expressed as the first-order reaction formula such as model 1. However, the initial concentration of 1.5 mmol·L$^{-1}$ was very close to the solubility, so it was a very small precipitate that was difficult to measure the change in concentration in. In addition, since the coefficient of determination of the model equation approaches 99%, this first-order reaction model equation was considered to be able to simulate the ferrous oxalate precipitation behavior very accurately.
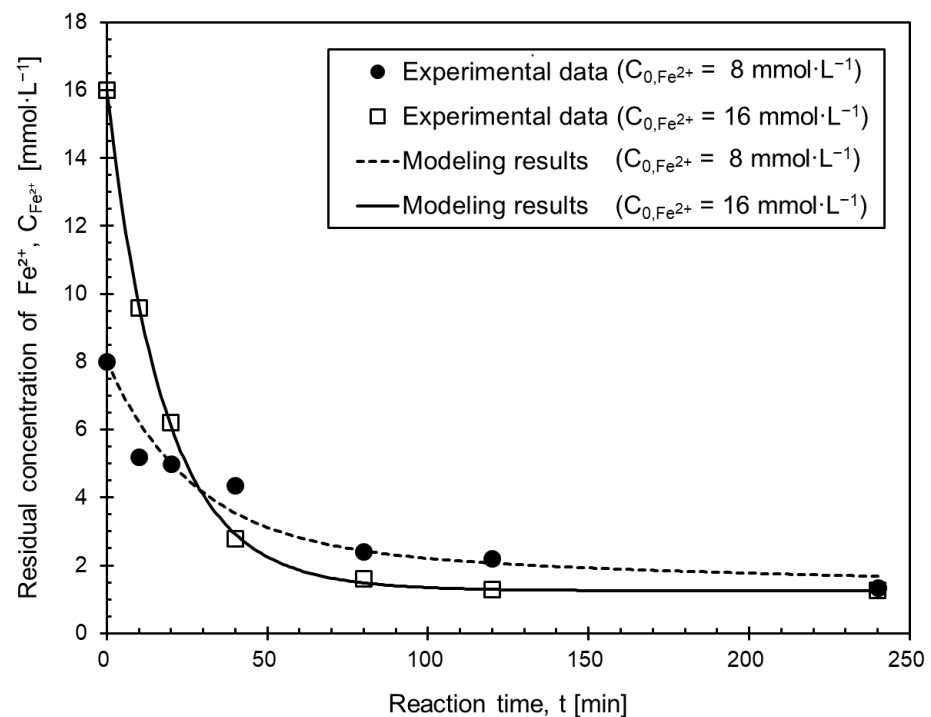
**Figure 8.** Experimental and modeling results of the ferrous oxalate precipitation behavior for initial concentrations of ferrous ions ($C_{0,Fe^{2+}}$) of 8 ($\bullet$) and 16 ($\square$) mmol·L$^{-1}$, by using ferrous ammonium sulfate system at $C_{OA}$ = 60 mmol·L$^{-1}$ and 25 °C.

## 4. Conclusions

Through an experimental kinetic study on the ferrous oxalate precipitation depending on the concentrations of both oxalic acid and ferrous ammonium sulfate, the following conclusions were obtained in the experimental range:

a.  The higher the initial ferrous concentration, the faster precipitation, due to the more precipitate particles which supplied particle growth sites.

b.  The change in oxalic acid concentration did not significantly affect the precipitation rate.

c.  The ferrous oxalate precipitation behavior could be modeled with a first-order response of the residual ferrous concentration.

# References

1.  Lee, B.-C.; Oh, W. Temperature and Concentration Dependencies of Chemical Equilibrium for Reductive Dissolution of Magnetite Using Oxalic Acid. *J. Nucl. Fuel Cycle Waste Technol. (JNFCWT)* **2021**, *19*, 187–196. [CrossRef]
2.  Kim, H.R.; Park, J.K.; Lee, S.I.; Oh, W.; Kim, J.; Kim, C.; Lee, B.-C. Kinetics of Reductive Dissolution of a Magnetite Specimen Using Oxalic Acid. *Processes* **2022**, *10*, 696. [CrossRef]
3.  Moon, J.; Kim, S.; Choi, W.; Choi, B.; Chung, D.; Seo, B. The Status and Prospect of Decommissioning Technology Development at KAERI. *J. Nucl. Fuel Cycle Waste Technol. (JNFCWT)* **2019**, *17*, 139–165. [CrossRef]
4.  Lee, S.O.; Tran, T.; Park, Y.Y.; Kim, S.J.; Kim, M.J. Study on the kinetics of iron oxide leaching by oxalic acid. *Int. J. Miner. Process.* **2006**, *80*, 144–152. [CrossRef]
5.  Lee, S.O.; Tran, T.; Jung, B.H.; Kim, S.J.; Kim, M.J. Dissolution of iron oxide using oxalic acid. *Hydrometallurgy* **2007**, *87*, 91–99. [CrossRef]
6.  Salmimies, R.; Mannila, M.; Juha, J.; Häkkinen, A. Acidic Dissolution of Magnetite: Experimental Study on The Effects of Acid Concentration and Temperature. *Clays Clay Miner.* **2011**, *59*, 136–146. [CrossRef]
7.  Salmimies, R.; Vehmaanperä, P.; Häkkinen, A. Acidic dissolution of magnetite in mixtures of oxalic and sulfuric acid. *Hydrometallurgy* **2016**, *163*, 91–98. [CrossRef]
8.  Manjanna, J.; Venkateswaran, G.; Sherigara, B.S.; Nayak, P.V. Dissolution studies of chromium substituted iron oxides in reductive-complexing agent mixtures. *Hydrometallurgy* **2001**, *60*, 155–165. [CrossRef]
9.  Won, H.-J.; Lee, W.-S.; Jung, C.-H.; Park, S.-Y.; Choi, W.-K.; Moon, J.-K. A Feasibility Study on the Decontamination of Type 304 Stainless Steel by N2H4 Base Solution. *Asian J. Chem.* **2014**, *26*, 1327–1330. [CrossRef]
10. Müller, H.; Bourcet, L.; Hanfland, M. Iron(II)oxalate Dihydrate—Humboldtine: Synthesis, Spectroscopic and Structural Properties of a Versatile Precursor for High Pressure Research. *Minerals* **2021**, *11*, 113. [CrossRef]
11. Li, C.; Ning, Y.; Yan, T.; Zheng, W. Studies on nucleation and crystal growth kinetics of ferrous oxalate. *Heliyon* **2019**, *5*, e02758. [CrossRef] [PubMed]
12. Abdel-Ghafar, H.M.; Ibrahim, M.A.M.; El-Shall, H.; Ismail, A.K. Innovative findings about ferrous oxalate dihydrate crystallization in simulated dihydrate phosphoric acid product. *Water Sci. Technol.* **2018**, *77*, 2940–2945. [CrossRef] [PubMed]
13. Abdel-Ghafar, H.M.; Abdel-Aal, E.A.; Ibrahim, M.A.M.; El-Shall, H.; Ismail, A.K. Studying nucleation aspects and morphology of iron (II) oxalate dihydrate crystals in water and diluted phosphoric acid media. *Egypt. J. Pet.* **2018**, *27*, 1235–1240. [CrossRef]
14. Abdel-Ghafar, H.M.; Abdel-Aal, E.A.; Ibrahim, M.A.M.; El-Shall, H.; Ismail, A.K. Purification of high iron wet-process phosphoric acid via oxalate precipitation method. *Hydrometallurgy* **2019**, *184*, 1–8. [CrossRef]
15. Xiao, Y.; Sun, T.; Zhao, Y.-H. Experimental Study on Preparation of Ferropericlase by Oxalate Coprecipitation. *Minerals* **2020**, *10*, 179. [CrossRef]
16. Santawaja, P.; Kudo, S.; Tahara, A.; Asano, S.; Hayashi, J.-I. Dissolution of Iron Oxides Highly Loaded in Oxalic Acid Aqueous Solution for a Potential Application in Iron-Making. *ISIJ Int.* **2021**. [CrossRef]
17. Ghasemi, S.; Rafiei, N.; Heidarpour, A. Theoretical analysis and experimental Validation of selective oxalate precipitation. *Miner. Process. Extr. Metall.* **2020**, *131*, 79–84. [CrossRef]
18. Wikipedia. Available online: en.wikipedia.org/wiki/Iron(II)_oxalate (accessed on 15 November 2022).